Biochimica et Biophysica Acta 1787 (2009) 721–729

Contents lists available at ScienceDirect

Biochimica et Biophysica Acta

journal homepage: www.elsevier.com/locate/bbabio

Review

Ion transport and energy transduction of P-type ATPases: Implications from electrostatic calculations

Christian Weidemüller, Karin Hauser *

Institut für Biophysik, Johann Wolfgang Goethe-Universität Frankfurt, Max-von-Laue-Str.1, 60438 Frankfurt am Main, Germany

ARTICLE INFO

Article history:
Received 9 December 2008
Received in revised form 13 February 2009
Accepted 17 February 2009
Available online 2 March 2009

Keywords:
P-type ATPase
Ca^{2+}-ATPase
Na^+/K^+-ATPase
Proton countertransport
Energy transduction
Electrostatic calculations

ABSTRACT

This paper summarizes our present electrostatic calculations on P-type ATPases and their contribution to understand the molecular details of the reaction mechanisms. One focus was set on analyzing the proton countertransport of the sarcoplasmic reticulum Ca^{2+}-ATPase (SERCA1a). Protonation of acidic residues was calculated in dependence of pH for different enzyme states in the reaction cycle of the Ca^{2+}-ATPase. We proposed that the acidic Ca^{2+} ligands Glu 771, Asp 800 and Glu 908 participate in the proton countertransport whereas Glu 309 is more likely to serve as a proton shuttle between binding site I and the cytoplasm. Complementary to infrared measurements, we assigned infrared bands to specific Ca^{2+} ligands that are hydrogen bonded. Ion pathways were proposed based on the calculations and structural data. Another focus was set on analyzing the energy transduction mechanism of P-type ATPases. In accordance to electrophysiological experiments, we simulated an electric field across the membrane. The impact of the electric field was studied by an accumulated number of residue conformational and ionization changes on specific transmembrane helices. Our calculations on the Ca^{2+}-ATPase and the Na^+/K^+-ATPase indicated that the highly conserved transmembrane helix M5 is one structural element that is likely to act as energy transduction element in P-type ATPases. Perspectives and limitations of the electrostatic calculations for future computational studies are pointed out.

1. Introduction

P-type ATPases form a large family of ubiquitous membrane proteins that pump ions across either cell membranes or membranes of intracellular organelles such as the endoplasmic or sarcoplasmic reticulum. Those ion pumps transport different kinds of cations ranging from H^+, Na^+, K^+, Ca^{2+} to heavy metals such as Cu^{2+}, Cd^{2+} and Hg^{2+} [1,2]. The active transport is driven against a concentration gradient by using the energy derived from ATP. Approximately 30% of the ATP produced in mammalian cells are consumed by P-type ATPases [3]. The formation of the covalent aspartyl-phosphorylated intermediate distinguishes P-type ATPases from other active transporters like F-, V-, and ABC-ATPases [4]. As they become transiently phosphorylated during the reaction cycle, they are termed as "P-type". After binding and hydrolysis of ATP, the terminal phosphate group of ATP is attached to a conserved aspartic acid of the protein. This aspartic acid is located in a 7 amino acid sequence, the most common motif for P-type ATPases is DKTGTLT [5]. Prominent members of P-type ATPase family include the Ca^{2+}-ATPase and the Na^+/K^+-ATPase. The Ca^{2+}-ATPase of skeletal muscle sarcoplasmic reticulum (SERCA1a) induces the relaxation of muscle cells. It actively pumps calcium back into the sarcoplasmic reticulum (SR) that has been released from the SR into the muscle cells via Ca^{2+}-release channels when the muscle is contracted. Calcium ions are transported from the cytoplasmic to the SR lumenal side of the membrane reducing the cytoplasmic Ca^{2+} to concentrations less than 0.1 μM. 2 Ca^{2+} ions are transferred per ATP hydrolyzed [6,7] and 2–3 H^+ are countertransported [8]. The Ca^{2+}-ATPase is an electrogenic pump although no H^+ gradient is built up across the SR membrane because it is leaky to H^+. The Na^+/K^+-ATPase is a P-type ATPase that is composed of 3 subunits. Ion transport and ATP binding take place in the α-subunit that is homologous to the single subunit Ca^{2+}-ATPase. It is an electrogenic pump exporting 3 Na^+ ions and importing 2 K^+ ions in each reaction cycle thereby maintaining the electrochemical gradient of Na^+ and K^+ across the plasma membrane of most animal cells. Understanding the reaction mechanism of P-type ATPases has additional pharmaceutical relevance, for example heart drugs target the Na^+/K^+-ATPase [9,10] or gastroesophageal acid reflux drugs target the gastric H^+/K^+-ATPase, another P-type ATPase family member [11,12].

The basic transport mechanism of P-type ATPases is commonly described by the classical E1/E2 model based on cyclic changes between two main conformational enzyme states, termed as E1 and E2 [13–15]. These changes are coupled to the vectorial ion transport.

Abbreviations: BHQ, 2,5-di-*tert*-butyl-1,4-dihydroxybenzene; E1P·2Ca^{2+}, ADP-sensitive phosphoenzyme; E2(TG), Ca^{2+} free ATPase with thapsigargin bound; E2P, ADP-insensitive phosphoenzyme; E2(TG + MgF_4^{2-}), the E2P analog structure obtained with MgF_4^{2-}; MCCE, multiconformation continuum electrostatics; SR, sarcoplasmic reticulum; TG, thapsigargin

* Corresponding author. Tel.: +49 69 798 46 407; fax: +49 69 798 46 423.
E-mail address: hauser@biophysik.uni-frankfurt.de (K. Hauser).

0005-2728/$ – see front matter © 2009 Elsevier B.V. All rights reserved.
doi:10.1016/j.bbabio.2009.02.015

The binding and hydrolysis of ATP provides the energy to drive this active ion transport against the concentration gradient at the membrane. The basic steps in the reaction cycle are assumed to be the same in all P-type ATPases and to be assisted by a similar structural architecture. Ten transmembrane helices (M1–M10) form the ion translocation site and are linked to three cytoplasmic domains where nucleotide binding and phosphorylation take place. The cytoplasmic domains are divided into the nucleotide binding (N)-, the phosphorylation (P)-, and the actuator (A)-domain. The N-domain binds ATP, the P-domain contains the phosphorylation site with the conserved residue Asp 351, and the A-domain is assumed to act as actuator of the gates that regulate ion binding and release [16]. The ion binding sites are located quite at the center of the transmembrane domain. Some of the 10 transmembrane helices (M2–M5) have long extensions into the cytoplasmic head part that are termed as stalks (S2–S5). The Ca^{2+}-ATPase is structurally and functionally the best characterized P-type ATPase so far and thus advanced to be the model protein of the whole P-type ATPase family for understanding the transport cycle. Fig. 1 shows the E1/E2 reaction model exemplarily for the Ca^{2+}-ATPase. Two cytosolic Ca^{2+} bind sequentially and cooperatively to the two high affinity Ca^{2+} binding sites [6,17,18] which release 2 [18–23] or 3 [24] H^+ to the cytoplasm at pH 6 ($E1{\cdot}2Ca^{2+}$). The Ca^{2+} binding initiates the ATP binding to the catalytic site ($E1{\cdot}ATP{\cdot}2Ca^{2+}$) and enables ATP to phosphorylate the Ca^{2+}-ATPase at Asp 351 forming a Ca^{2+} occluded high-energy state ($E1P{\cdot}2Ca^{2+}$). Several phosphoenzyme intermediate states are formed consecutively, some of them have been crystallized up to now (for an overview see [7]), and others are postulated by mutational studies [25]. The E2P intermediate dephosphorylates by the reaction with water and its formation is accompanied by the release of Ca^{2+} into the SR lumen. Even high lumenal Ca^{2+} concentrations do not inhibit the lumenal release of Ca^{2+} from the phosphoenzyme [26,27]. The Ca^{2+} release is accompanied by the uptake of 2–3 H^+ from the SR lumen [19,24,28,29]. Hydrolysis of E2P to E2 and regeneration to the high affinity binding sites (E1) completes the reaction cycle. All steps are reversible. E1 and E2 are often interpreted as the two main conformational states of the enzyme with different orientation and affinity of the Ca^{2+} binding sites. This view of intermediate states has also been questioned and a switch mechanism has been proposed instead in which the Ca^{2+} binding and the Ca^{2+} release switch the reaction specificity of the phosphorylation site whereas phosphorylation and dephosphorylation switch the accessibility and affinity of the Ca^{2+} sites [30]. However, the coordinated affinity change at the transport sites is the key to active transport as the cytoplasmic calcium ions are bound with μM affinity and released to the lumen with mM affinity [31]. Also the coupling between the phosphorylation site and the Ca^{2+} binding sites is necessary for efficient Ca^{2+} pumping. The chemical free energy of the ATP hydrolysis is used with an efficiency up to 100% that is 39–42 kJ/mol [32,33]. The transport is accompanied with structural changes [7,16,31,32]. The transition from the calcium bound to the calcium free state disrupts the Ca^{2+} binding sites by the movement of the coordinating residues. The coordinating residues are located on the helices M4, M5, M6 and M8. According to the crystal structures, the transmembrane helices M1–M6 move during the transport cycle whereas M7–M10 keep their positions and anchor the protein in the membrane [16,32]. However, the most significant structural changes occur in the cytoplasmic head part. The domains move considerably between an open arrangement of the A-, P-, and N-domains in the $E1{\cdot}2Ca^{2+}$ state and a compact conformation in all other intermediates.

The variety of structural and functional studies of P-type ATPases is constantly summarized in reviews, e.g. for the Ca^{2+}-ATPase in [7,11,16,31,32,34–37] and for the Na^+/K^+-ATPase in [5,38–42]. The number of crystal structures of the Ca^{2+}-ATPase increased tremendously in the last years and atomic coordinates of most transport intermediates or of analog states are now available [43–50]. The present status of solved Ca^{2+}-ATPase structures has been summarized in a recent review [7]. A crystal structure of the Na^+/K^+-ATPase E2·P-state has also been solved lately [51]. The availability of structural data provides the accessibility for computational analysis. However, the molecular system is fairly large (994 residues; ~15 800 atoms including hydrogens) what remains a challenge for simulations. The computational and theoretical studies on P-type ATPases that have been performed so far addressed questions as e.g. the binding of the ions or of inhibitors [52,53], domain motions [54–57], ion transport and gating mechanisms [58,59] or heat flux accompanying the ion transport [60,61]. Most of the present computational studies on P-type ATPases use molecular dynamics, docking and normal mode analysis approaches. Continuum electrostatic calculations have been performed to study the protonation of binding site residues of the Ca^{2+}-ATPase [62,63]. Our studies focus on the electrostatic properties which are important for the ion transport as well as for the energy transduction mechanism. Compared to continuum electrostatic calculations, the multiconformation continuum electrostatics (MCCE) approach additionally includes various side chain orientations that are sampled simultaneously with the ionization states of the residues. Thus a conformational flexibility is included explicitly and furthermore, the coupling of ionization and side chain conformer changes can be monitored.

In this report, we summarize the results of our present simulation studies on ion transport and energy transduction of P-type ATPases [64–69]. Our electrostatic simulations have been performed complementary to experimental studies. We analyzed the proton countertransport of the Ca^{2+}-ATPase. The Ca^{2+} coordinating residues were studied in particularly. Their pK_a-value, protonation state and side chain orientation were calculated in dependence of pH for different enzyme states in the transport cycle. The calculations were performed in combination with infrared studies and contributed to assign infrared bands to specific Ca^{2+} residues that get protonated upon Ca^{2+} release. Ligands were identified that are likely to be involved in the proton countertransport and their functional role within the proton translocation was proposed.

The energy transduction was studied motivated by voltage-clamp fluorometry experiments that induce the reaction cycle by applying voltage jumps across the membrane and that localize helix conformational changes on specific helices during the transport cycle [70]. We simulated an electric field across the membrane, calculated the conformational and ionization changes of residues and analyzed the impact of an electric field on each transmembrane helix for the Ca^{2+}-ATPase and the Na^+/K^+-ATPase. Although only a qualitative analysis can be performed, the electrostatic calculations showed that the transmembrane helices respond differently to the electric field in terms of conformer changes and thus support the hypothesis that specific transmembrane helices are likely to act as energy transduction elements.

2. Methods

2.1. Multiconformation continuum electrostatics

Multiconformation continuum electrostatics (MCCE) is a hybrid method that combines continuum electrostatics and molecular mechanics. Details of the MCCE program can be found, e.g. in [71,72]. Several MCCE studies on proteins have been reported, e.g. [73–78]. Titration curves respectively pK_a-values as well as side chain orientations are calculated for each residue in dependence of pH. Energy terms that shift the pK_a of a residue in solution to its pK_a in the protein environment can be identified. Each residue is represented by a set of conformers that differ in ionization, side chain orientation (rotamer) and hydrogen positions. Rotamers are constructed systematically by rotating rotatable side chain bonds with variable angle increment. Steric clashes and strong interactions reduce the total number of rotamers that are included in the calculations. The protein

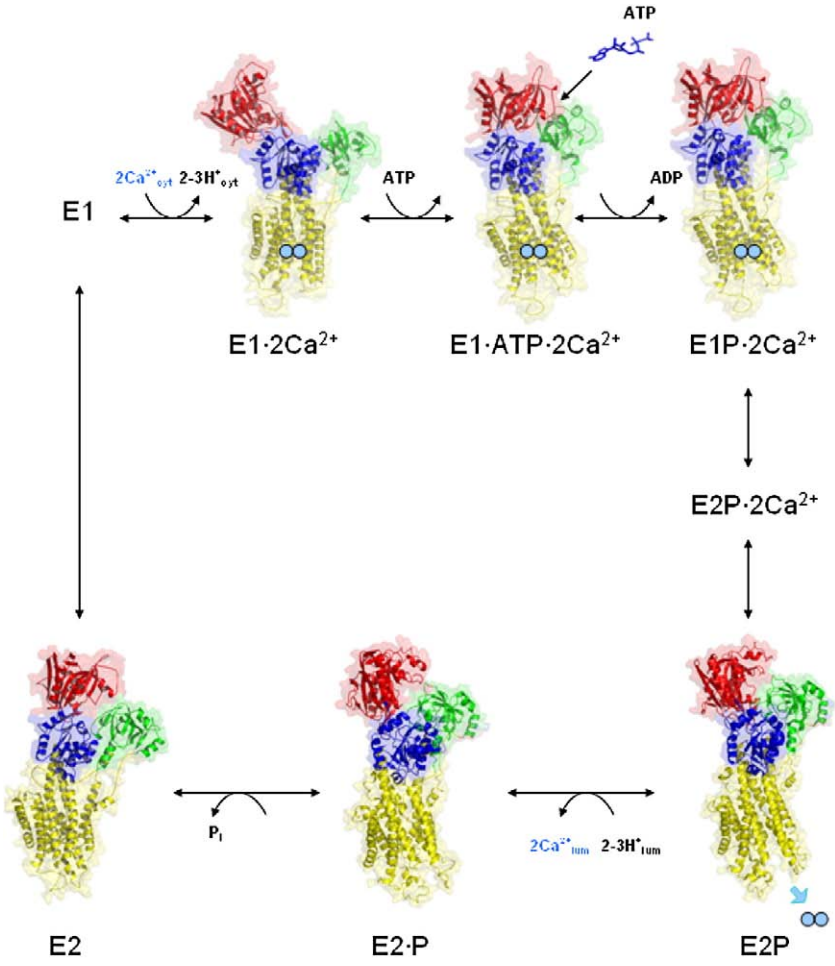

Fig. 1. The basic reaction cycle for the Ca^{2+}-ATPase. After binding of 2 cytosolic Ca^{2+} ions ($E1 \cdot 2Ca^{2+}$), ATP binds ($E1 \cdot ATP \cdot 2Ca^{2+}$), gets hydrolyzed and enables phosphorylation. Several phosphoenzyme intermediates are formed consecutively ($E1P \cdot 2Ca^{2+}$, $E2P \cdot 2Ca^{2+}$, E2P, $E2 \cdot P$). The Ca^{2+} ions are released into the SR lumen and 2–3 H^+ are taken up from the SR lumen. After dephosphorylation (E2), the enzyme recovers to the conformation with high affinity Ca^{2+} binding sites (E1). See text for more details. High resolution structures (shown as cartoons) are presently available for almost all enzyme states. The structural data used for the figure are the pdb-entries 1SU4 [43], 1T5S [97], 1T5T [97], 3B9B [49], 1WPG [46] and 2AGV [63]. The cytoplasmic domains are colored in blue (P), red (N) and green (A), and the transmembrane domain in yellow.

backbone remains fixed. Electrostatic and non-electrostatic interactions are calculated between all conformers. Protein microstates are created by choosing one conformer per residue. The free energy of each microstate is the sum of several energy terms including the reference $pK_{a,sol}$ of the residue in solution, conformer self energies, interactions with the backbone and other fixed conformers, and pairwise electrostatic and non-electrostatic interactions between conformers [71,74]. The microstates are subjected to a Monte Carlo sampling. Calculation outcome is the pH-dependent occupancy of all conformers that are assigned to a residue. All electrostatic interactions are calculated with the program Delphi [79] based on the linear Poisson–Boltzmann equation. For the protein, the dielectric constant $\varepsilon=4$ was chosen, while 80 was used for the solvent. PARSE parameters provide atomic charges and radii [80]. Torsion and Lennard–Jones parameters were previously reported [72].

2.2. Ionic capacitor to simulate an electric field

We implemented a transmembrane electric field into the MCCE method by inserting ions above and below the transmembrane region of the protein at the membrane boundaries. Thus the ions act like capacitor plates that generate a homogenous electric field. The electric field strength can be varied by choosing a different number and charge of the inserted ions or by varying the capacitor plates' distances. The impact of the electric field on individual transmembrane helices of the ATPase was analyzed by summing up the conformer changes per helix that are induced by the electric field. A typical simulation setup containing the ATPase, a modeled membrane and the ionic capacitor is shown in Fig. 4. To avoid counting changes that are induced for

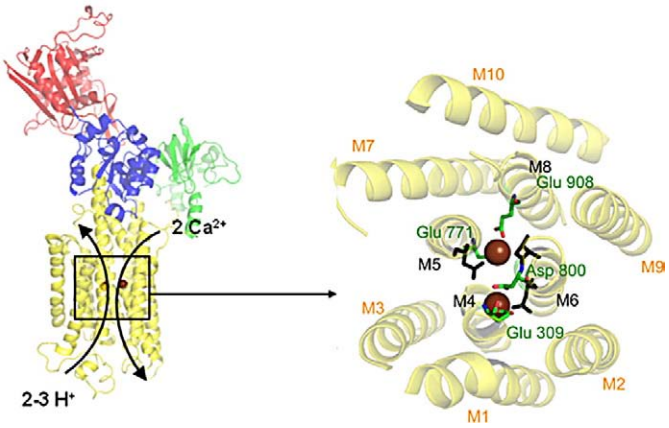

Fig. 2. The ion binding sites of the Ca^{2+}-ATPase. Left: localization within the whole protein. The cytoplasmic domains are colored in blue (P), red (N) and green (A), and the transmembrane domain in yellow. Right: Top view of the transmembrane domain. The Ca^{2+} ions (brown) are coordinated by the Ca^{2+} ligands (shown as sticks) that are located on the transmembrane helices M4, M5, M6 and M8. The four acidic Ca^{2+} ligands (Glu 309, Glu 771, Asp 800, Glu 908) that are prime candidates to be involved in the proton countertransport are highlighted in green.

example by steric perturbations of the ionic capacitor, MCCE calculations have been performed with and without an applied electric field, i.e. the capacitor was placed into the simulation setup once with ions and once with atoms. The most occupied conformer was extracted for each residue in each simulation setup (with and without applied electric field). Only those residues were counted in the final evaluation that changed when the electric field was applied and all conformer changes were summed up for each transmembrane helix M1–M10. Hydrogen bond orientation changes of an angle increment of less than 10° have been neglected. The conformer changes were distinguished in rotamer and ionization changes as shown exemplarily in Fig. 5. Typical parameters for the ionic capacitor can be found in Section 2.3.

2.3. Simulation details

Simulation details for the proton countertransport [64–67] and the energy transduction [68,69] were reported previously. Here, we provide the simulation parameters for the new calculations with the recently solved 3.5 Å crystal structure (3B8E) of the E2·P-state of the Na^+/K^+-ATPase [51]. Mg^{2+}, MgF_4^{2+} and Rb^+ ions, PC1 (1,2-diacyl-sn-glycero-3-phosphocholine) and crystal water molecules were deleted for the calculations. Cavities that are large enough for water molecules were treated with a continuum water approximation using $\varepsilon = 80$. The transmembrane domain (residues 70–150; 250–360; 740–1024) and the helices M1–M10 of the Na^+/K^+-ATPase were assigned according to the Swiss-Prot Database [81]. The protein was embedded into a POPC (1-palmitoyl 2-oleoyl phosphatidylcholine) bilayer consisting of 128 lipids solvated with 35035 water molecules. The generation of the membrane was performed with VMD [82] and the gap between the membrane and the protein was closed with a molecular dynamics simulation using NAMD [83] with the CHARMM27 force field. The total molecular system consisted of 137796 atoms and was coupled to a temperature bath at 310 K. After the protein/membrane complex generation, the hydrogens were deleted since they are regenerated in MCCE. The POPC bilayer was parameterized as neutral cofactor with no rotamers assigned. For the ionic capacitor, 100 atoms with a van-der-Waals radius of 1.7 Å were inserted in rows above and below the transmembrane region at the membrane boundaries. The dimensions of the capacitor plates were roughly 50 Å × 50 Å and the distance between the plates 60 Å. The electric field strength was set to $2.4 \cdot 10^{11}$ V/m with ion charges of +9/−9 a.u. The whole simulation setup (ATPase, membrane and ionic capacitor) was implemented in MCCE and the calculations were performed with the program version "mcce1.0".

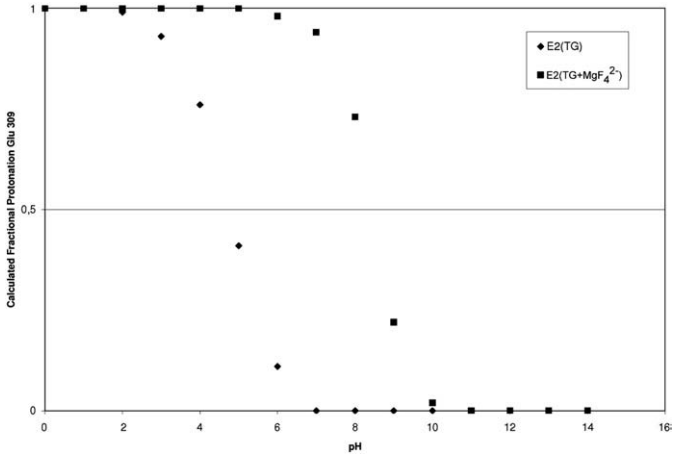

Fig. 3. Calculated titration curve of Glu 309 in the E2(TG) and the E2(TG + MgF_4^{2-}) state of the Ca^{2+}-ATPase. The pK_a-values have been calculated to be 4.7 in E2(TG) and 8.4 in E2(TG + MgF_4^{2-}). The difference was attributed to the different local backbone structure around Glu 309 in the crystal structures. The calculations indicated large conformational flexibility of the Glu 309 side chain.

3. Proton countertransport of the Ca^{2+}-ATPase

It is well established that the transport of Ca^{2+} ions across the membrane is associated with a proton countertransport from the SR lumen to the cytoplasm [20,84,85]. The basic reaction cycle of the Ca^{2+}-ATPase is shown in Fig. 1. When the two cytosolic Ca^{2+} ions have bound to the Ca^{2+}-ATPase (E1·2Ca^{2+}), protons are released into the cytoplasm and the nucleotide ATP binds to the N-domain, gets hydrolyzed and phosphorylates the Ca^{2+}-ATPase at Asp 351. The phosphoenzyme then converts from an ADP-sensitive E1P·2Ca^{2+} to an ADP-insensitive form E2P and Ca^{2+} is released to the SR lumen against a concentration gradient. Protons are taken up from the lumenal side of the membrane and are released to the cytoplasmic side of the membrane upon Ca^{2+} rebinding. The proton uptake and release reactions constitute the proton countertransport of the Ca^{2+}-ATPase. The two calcium binding sites are located in the transmembrane region at helices M4, M5, M6 and M8 [36]. Calcium coordination at site I is provided by the side chain oxygens of Asn 768 and Glu 771 from M5, Thr 799 and Asp 800 from M6, and Glu 908 from M8. At site II, the Ca^{2+} ion is coordinated by contributions from both side chain and backbone oxygens, side chain oxygens of Asn 796 and Asp 800 from M6 and Glu 309 from M4, and backbone oxygens of Val 304, Ala 305 and Ile 307 from M4. Asp 800 is part of site I and site II and coordinates both Ca^{2+} ions. Fig. 2 shows the location of the binding site and all ligands that provide side chain oxygens. Calcium ions and protons are thought to compete for the same binding sites as protons are likely to be required for stabilization of the Ca^{2+}-ATPase structure by partly neutralizing the empty binding sites [16]. There are different assumptions if each Ca^{2+} competes with one H^+ [18,22,23] or the protons have to be released before the first Ca^{2+} binds [19,21,23,24]. Prime candidates for binding the countertransported protons are the acidic residues of the binding sites [18,20–23,84]. Four of the binding site residues contain carboxyl groups: Glu 309 (binding site I), Glu 771 (binding site II), Asp 800 (sites I and II) and Glu 908 (site I) that are marked with colors in Fig. 2. The proton countertransport is reduced by increasing the luminal pH from 6 to 8 [86]. Thus the residues that participate in the proton countertransport should be less protonated at high pH.

3.1. Role of acidic Ca^{2+} ligands in the proton countertransport

To analyze the participation of the acidic Ca^{2+} ligands (Glu 309, Glu 771, Asp 800, Glu 908) in the proton countertransport, we calculated their pK_as respectively fractional protonation in dependence of pH for different enzyme states, i.e. the Ca^{2+}-bound state E1·2Ca^{2+} and the Ca^{2+} free states, E2 with bound thapsigargin (E2(TG)) and the E2P analog state with MgF_4^{2-} (E2(TG + MgF_4^{2-})) [67]. Side chain conformation and protonation are simulated simultaneously in MCCE calculations, thus both changes are monitored explicitly as a function of pH. The acidic ligands should be deprotonated in the Ca^{2+}-bound state and protonated in the Ca^{2+} free states at physiological pH if they compete for the Ca^{2+} ions and protons. If additionally involved in the proton countertransport, they should deprotonate in the Ca^{2+} free states at high pH. Experimentally determined apparent pK_a-values are near 7.5 for lumenal proton binding of countertransported residues [19,24,86].

Our calculations indicated that at physiological pH all acidic ligands were ionized in the Ca^{2+}-bound state. Glu 771, Asp 800 and Glu 908 were protonated in the Ca^{2+} free states E2(TG) and E2(TG + MgF_4^{2-}). Glu 771, Asp 800 and Glu 908 were protonated. Glu 771 and Glu 908 had calculated pK_a-values larger than 14 in E2(TG) and E2(TG + MgF_4^{2-}), whereas Asp 800 titrated with calculated pK_a-values near 7.5 [64,67]. Glu 309 had very different pK_a-values in the Ca^{2+} free states: 8.4 in E2(TG + MgF_4^{2-}) and 4.7 in E2(TG) as shown in Fig. 3. We

attribute the striking pK_a difference to the different local backbone structure around Glu 309 in the crystal structures. The amide oxygen faces outwards in the E2(TG + MgF_4^{2-}) structure whereas it faces inwards in the E2(TG) structure and thus directs the C_α–C_β bond of the Glu 309 backbone differently. The crystal structure backbone influences the calculated pK_a-values because conformational degrees of freedom are only given to the side chains whereas the backbone remains fixed in the MCCE approach. However, our calculations showed that the protonated Glu 309 side chain can orient in opposite directions in both structures, one conformation oriented inwards towards the other Ca^{2+} ligands and one conformation oriented outwards towards a channel inside the protein that seems to be in contact with the cytoplasm [67]. This indicates that Glu 309 can switch between a high and a low pK_a mode depending on the local backbone conformation. Upon deprotonation at higher pH, Glu 309 adopted completely the outwardly orientated side chain conformation. The contact of Glu 309 with the cytoplasm in E2(TG + MgF_4^{2-}) makes this residue unlikely to bind lumenal protons in E2P. Instead it might serve as a proton shuttle between Ca^{2+} binding site I and the cytoplasm. Outward movement of the Glu 309 side chain might also be a possible trigger for Ca^{2+} release along an exit path between transmembrane helices M1, M2, and M4 [67]. Glu 771, Asp 800 and Glu 908 are proposed to take part in proton countertransport. Without the participation of Glu 309, our calculated number of countertransported residues is between 2 and 3, which compares favorably with experimental values at physiological pH and below [64,67].

3.2. Protonation and hydrogen bonding of acidic Ca^{2+} ligands — band assignment of infrared bands with electrostatic calculations

Protonation of the acidic Ca^{2+} ligands were studied by electrostatic calculations in combination with time-resolved Fourier transform infrared (FTIR)-measurements [64–67]. FTIR-difference spectroscopy is predestinated to monitor the protonation of carboxyl groups during protein reactions [87,88]. Thus the protonation of Glu and Asp side chains can be followed since the absorption of the corresponding vibrations are well distinguishable from the absorption of other amino acids. However, the assignment to individual groups within the protein needs additional information, e.g. from induced spectral changes due to isotopic labeling or mutation. We used MCCE calculations to assign infrared bands to individual acidic Ca^{2+} ligands [64,65].

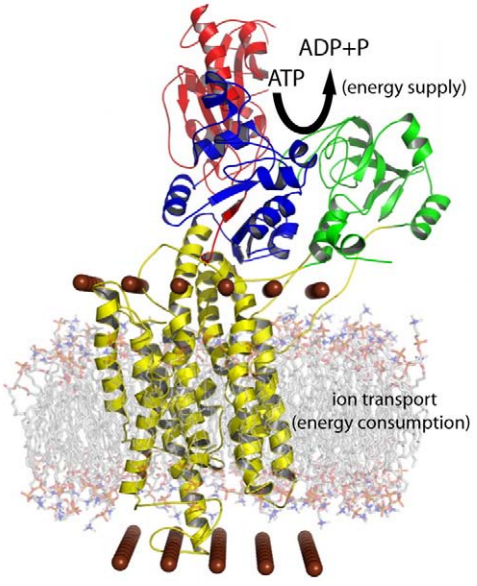

Fig. 4. Simulation setup with an "ionic capacitor". The energy derived from ATP is supplied in the cytoplasmic head part and has to be transferred to the transmembrane part where the ion transport takes place. Electrophysiological experiments indicate that the energy transduction is regulated by specific structural elements. We simulated an electric field across the membrane by placing ions above and below the transmembrane part of the protein (here: Na^+/K^+-ATPase). The conformer changes induced by the electric field were evaluated for each transmembrane helix. The modeled lipid membrane is shown in grey.

The pH dependence of C=O infrared bands of the Ca^{2+} free phosphoenzyme state E2P gives direct experimental evidence for carboxyl groups that get protonated upon Ca^{2+} release [65]. At least three of the infrared signals from protonated carboxyl groups of E2P were pH-dependent with pK_a-values near 8.3. One infrared band was characteristic for non-hydrogen bonded carbonyl groups whereas two other infrared bands were characteristic for hydrogen bonded carbonyl groups. They were thus assigned to H^+ binding residues, some of which are involved in H^+ countertransport. Bands without pH dependence were not attributed to Ca^{2+}/H^+ exchange [65]. With our MCCE calculations on E1·2Ca^{2+} and E2P analog E2(TG + MgF_4^{2-}) we assigned the infrared bands to specific residues and analyzed whether or not the carbonyl groups of the acidic Ca^{2+} ligands were hydrogen bonded. The pH dependence of the measured C=O bands was correlated to the calculated fractional protonation of the acidic Ca^{2+} ligands. The calculated occupancy of the various side chain rotamers was used to analyze possible hydrogen bonding patterns. Our calculations indicated considerable conformational heterogeneity of the acidic Ca^{2+} ligands in the Ca^{2+} free state E2(TG + MgF_4^{2-}) which allows various hydrogen bonding patterns. The carbonyl groups of Glu 771, Asp 800 and Glu 908 were found to be hydrogen bonded and thus to contribute to the lower wavenumber bands. The carbonyl group of some Asp 800 conformers was left without hydrogen bonding partner and thus assigned to contribute to the higher wavenumber band [65].

3.3. Ion pathways

Ion pathways were proposed based on our calculations and structural data [67]. The above described heterogeneity of Glu 309 supports a Ca^{2+} gating function of this residue towards the cytoplasm and it might also be important for the release of Ca^{2+} from the phosphoenzyme to the SR lumen. Ca^{2+} release is likely to be triggered by an outward movement of the Glu 309 side chain away from the Ca^{2+} binding sites. Exit to the cytoplasmic side is blocked by the outwardly oriented Glu 309 side chain and other residues. Exit to the lumen seems to be possible by a channel that is mainly formed by residues in transmembrane helices M1, M2 and M4. Most of the steric constraints of the Ca^{2+} channel are between transmembrane helices M1 and M4 or M2 and M4. This indicates that the channel can be opened and closed by movements of helices M1 and M2 relative to M3 and M4. Movements of the transmembrane helices M1 and M2 relative to M3 and M4 are a reoccurring theme in the structural reorganizations that take place during Ca^{2+} pumping [46]. In E1 · 2 Ca^{2+}, M1 and M2 have moved down towards the SR lumen with respect to M3 and M4 and adopt a different position with respect to M4. This disrupts the Ca^{2+} exit path.

Proton pathways in the Ca^{2+} bound and Ca^{2+} free states were also suggested by the analysis of crystal structures to which water molecules were added [66]. In the Ca^{2+} bound state E1·2 Ca^{2+}, one of the proposed Ca^{2+} entry paths was suggested to operate additionally or alternatively as proton pathway. In analog states of the ADP-insensitive phosphoenzyme E2P and in the Ca^{2+} free state E2, the proton path leads between transmembrane helices M5 to M8 from the lumenal side of the protein to the Ca^{2+} binding residues Glu 771, Asp 800 and Glu 908. We suggested that separate proton and Ca^{2+} pathways enable rapid (partial) neutralization of the empty cation binding sites. For this reason, transient protonation of empty cation binding sites and separate pathways for different ions are advantageous for P-type ATPases in general.

4. Energy transduction

P-type ATPases convert chemical energy, derived from the hydrolysis of ATP, into a vectorial mechanism for cation transport.

The coupling between the phosphorylation site and the ion binding sites occurs over a distance of more than 50 Å. A key question is how the phosphorylation site (where the energy is supplied) and the ion binding sites (where the energy is consumed) communicate with each other. Based on crystallographic data of the Ca^{2+}-ATPase, the most structural changes during the transport cycle occur in the cytoplasmic head part. The domains move considerably between an open arrangement of the A-, P-, and N-domains in the $E1 \cdot 2Ca^{2+}$ state and a compact conformation in all other intermediates. The transmembrane helices M7 to M10 keep their positions during the transport cycle and anchor the protein in the membrane [16,32] whereas transmembrane helices M1–M6 move. The M5 including the stalk is particularly long (60 Å) and ranges from the lumenal surface of the membrane via the cytoplasmic surface of the membrane till to the end of the P-domain. Besides the models proposing that conformational changes mechanically drive the ions to be transported in the transmembrane region, there are also models suggesting that the chemical energy of the ATP hydrolysis is transduced via well-defined charge-transfer pathways that connect the chemical reaction site with the site of ion binding [89]. On the basis of structural data of the Ca^{2+}-ATPase, Scarborough proposed two pathways, one running mainly along M4 and one mainly along M5 [89]. M5 and the subsequent extracellular M5–M6 loop are highly conserved among all P-type ATPases [38] and thus are likely to play a crucial role for coupling ATP hydrolysis to ion transport. The importance of helix M5 in functional rearrangement was suggested for the Na^+/K^+-ATPase [90] and the H^+/K^+-ATPase [91]. Charge translocation and transient currents of P-type ATPases have been extensively studied by electrical measurements that apply voltage jumps across the membrane to initiate the reaction cycle. Patch-clamp fluorometry experiments of the Na^+/K^+-ATPase showed that the extracellular end of helix M5 is involved in a voltage-dependent conformational change during the E1P–E2P transition and that this structural rearrangement is directly correlated to the main electrogenic step in the transport cycle [70]. Those measurements show further that only specific transmembrane helices respond to the electric field that is applied across the membrane and that these helices are likely to act as energy transduction elements in the reaction cycle.

In our computational study, we simulated an electric field across the membrane in accordance to the electrical measurements and studied its impact on the transmembrane region of a chosen enzyme state of the reaction cycle. The aim was to study if the electric field induces a selective helix activation in the transmembrane region. With our calculations we can evaluate the helix response to the electric field by changes in side chain conformation as well as changes in ionization of all residues in the transmembrane region. Since the protein backbone remains fixed in the MCCE approach, the detectable conformational changes are limited to changes in side chain conformations and cannot accomplish for larger protein movements. Thus we cannot simulate an enzyme transition in the reaction cycle as in the patch-clamp fluorometry experiments [70], but we can study the impact of an electric field on the conformational and ionization changes of side chains. Both might be crucial for the energy transduction mechanism, whether it is driven mechanically or by charge-transfer pathways or by a combination of both. The side chain conformational and ionization changes were evaluated per helix and it was analyzed whether there is a selectivity in helix response supporting the experimentally-driven hypothesis that the energy transduction mechanism is regulated by specific structural elements. Ionization changes might also be important to translocate energy from the cytoplasmic head to the transmembrane region, even if just indirectly by coupled ionization and conformational changes. Fig. 4 represents the simulation setup that contains the ATPase, a membrane and the ionic capacitor that we implemented into the MCCE method.

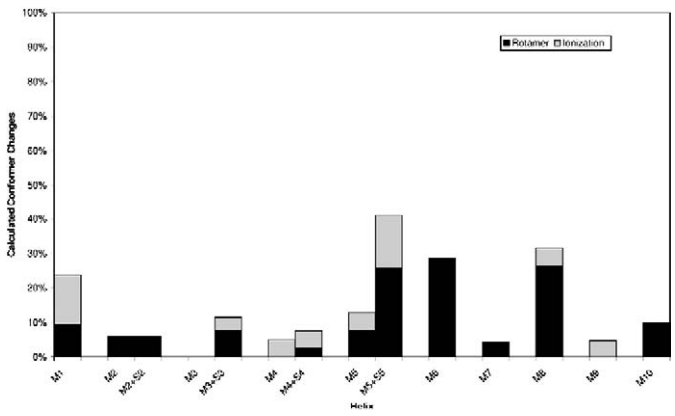

Fig. 5. Calculated conformer changes in the $E2 \cdot P$-state of the Na^+/K^+-ATPase due to an applied electric field. The fraction of conformer changes was evaluated for each transmembrane helix M1–M10. The helices extended by a stalk were separately evaluated and are shown with extra bars (M2 + S2 − M5 + S5). The conformer changes are distinguished in rotamer changes (black) and the ionization changes (grey).

4.1. Impact of an electric field studied by MCCE calculations

The results of MCCE calculation on the $E2 \cdot P$-state of the Na^+/K^+-ATPase are summarized in Fig. 5. The above described approach was used to simulate an electric field and the field-induced conformer changes were calculated for each of the transmembrane helices M1–M10. Helices that are extended by a stalk (M2–M5) were evaluated with and without including the stalk (S2–S5). The total number of helix residues varies between 19 and 21 without consideration of the stalks and between 19 and 39 when the stalks are included. For a better evaluation of the electric field impact on transmembrane helices with different lengths, the conformer changes were not given in absolute numbers but in percentage with respect to the total number of helix residues. The calculated conformer changes were further distinguished in rotamer and ionization changes.

M5 is the helix with the most conformer changes (40%) when the stalk region is included in the evaluation. 25% of rotamer changes and 15% of ionization changes are induced by the electric field. The importance of the stalk S5 for the intramolecular communication was already suggested by mutational studies [92]. M3 and M4 are other helices with stalks that show an increase when the stalk is included, but much less than M5, and the total number of conformer changes remains below 10%. M6 and M8 have a similar fraction of rotamer changes as compared to M5. M6 shows no ionization changes and M8 only 5%. M1 has a similar number of ionization changes as compared to M5, but less than 10% of rotamer changes. The location of the rotamer and ionization changes within each helix is illustrated in Fig. 6. It becomes obvious that conformer changes are induced on specific helices independently from the helix length. M4, for example, is only 3 residues shorter than M5 (when the stalk is included), but its number of conformer changes is below 10% as compared to 40% on M5. Although there are less changes on helix M4, this does not necessarily imply that M4 is not involved in the energy transduction. As mentioned above, the MCCE approach is restricted to side chain conformational changes whereas larger structural movements are not incorporated. Thus larger conformational changes might be essential for the participation of M4. This is indicated by our recent calculations where we combined electrostatic calculations with molecular dynamics simulations [69]. The number of conformer changes on M4 was significantly increased when structural rearrangements of the protein are included. The participation of M4 was also concluded by experimental studies [49,92,93]. Taken together, the most conformer changes were induced on M5 (with stalk included). The conformer changes consist of rotamer changes, but also of a significant amount of ionization changes. The conformer changes are evenly distributed

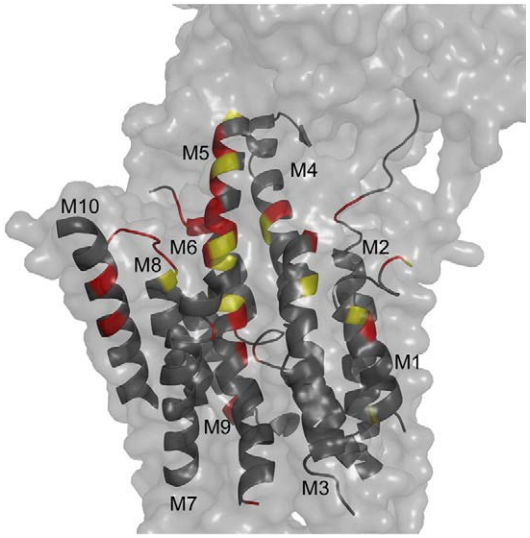

Fig. 6. Localization of conformer changes in the E2·P-state of the Na^+/K^+-ATPase due to an applied electric field. Shown is the distribution of rotamer changes (red) and ionization changes (yellow) along each of the transmembrane helices M1–M10. M5 is the helix with most conformer changes that are additionally evenly distributed along the whole helix.

along the whole helix as what has already been recognized by our previous calculations for the Ca^{2+}-ATPase [68].

4.2. Implications for the energy transduction of P-type ATPases

We calculated the conformer changes per transmembrane helix that are induced by an electric field across the membrane for the Ca^{2+}-ATPase, structural models of the Na^+/K^+-ATPase and in this study for the recently solved E2·P-state of the Na^+/K^+-ATPase [68,69]. Side chain conformational and ionization changes were evaluated and a selective activation of specific helices by the electric field became obvious. Certainly, our current approach has limitations as discussed below, but qualitatively it could be shown that individual helices showed more conformer changes than others. Our present calculations with different enzyme states of the Ca^{2+}-ATPase could identify M5 to be reproducible activated by an electric field [68]. Also our calculations on structural models of the Na^+/K^+-ATPase and the here presented calculations on the E2·P-state of the Na^+/K^+-ATPase identified M5 to be activated besides M6 and M8 [69]. The crucial role of M5 is even more emphasized when the stalk region is included in the evaluation. M5 is highly conserved in P-type ATPases. Our simulations support experimental results and indicate that the transmembrane helix M5 is likely to act as energy transduction element in the reaction cycle of P-type ATPases.

4.3. Limitations of the analysis

Our current simulation approach to study the impact of the electric field has limitations in tracking larger conformational changes. The backbone of the protein remains fixed in the MCCE approach and only the side chains are provided with a limited number of rotamers. Thus only conformational changes can be evaluated for side chains that are restricted to the supplied rotamers and no larger conformational changes of the whole protein can be followed. The fixed backbone and limited number of rotamers are certainly one reason why large electric field strengths have to be used in our simulation approach. In order to monitor rotamer changes, we had to use field strengths that are 100 to 1000-times larger than the physiological and experimentally applied electric fields. Other simulation studies analyzing electric fields across protein/membrane complexes use field strengths that are 10 to 100-times larger than the physiological transmembrane fields [94,95]. The limitations of the simulation approaches usually require high field strengths. It should also be noted that the physiological fields are not strictly homogeneous and can locally explore very high field strengths [95,96]. Taken together, a qualitative analysis is feasible with our present approach at relatively low computational costs as compared to other computational approaches on proteins of that size. Our ongoing studies combine electrostatics with molecular dynamics (MD), i.e. electrostatic calculations on MD snapshots, in order to overcome the limitations in conformational dynamics and to reduce the required electric field strengths.

5. Outlook

Ongoing and future computational studies on P-type ATPases include the combination of electrostatics with molecular dynamics. Ionization states of residues are calculated including the protein conformational dynamics. Cation transport, binding and pathways, but also the nucleotide binding and phosphorylation sites will be studied with an increasing number of high resolution atomic structures and complementary to experiments.

Acknowledgements

We thank Andreas Barth (Stockholm University) for the fruitful collaboration, Ernst Bamberg (Max-Planck Institute of Biophysics Frankfurt) for the valuable discussions and Marilyn Gunner (City College of New York) for providing and developing the MCCE code. Cluster access at the Frankfurt Center of Scientific Computing (CSC) and financial support of the Deutsche Forschungsgemeinschaft (SFB 472) are gratefully acknowledged.

References

[1] M.G. Palmgren, K.B. Axelsen, Evolution of P-type ATPases, Biochim. Biophys. Acta 1365 (1998) 37–45.
[2] J.V. Moller, B. Juul, M. le Maire, Structural organization, ion transport, and energy transduction of P-type ATPases, Biochim. Biophys. Acta 1286 (1996) 1–51.
[3] D.F.S. Rolfe, G.C. Brown, Cellular energy utilization and molecular origin of standard metabolic rate in mammals, Physiol. Rev. 77 (1997) 731–758.
[4] J.V. Moller, C. Olesen, A.-M.L. Jensen, P. Nissen, The structural basis for coupling of Ca^{2+} transport to ATP hydrolysis by sarcoplasmic reticulum Ca^{2+}-ATPase, J. Bioenerg. Biomembr. 37 (2005) 359–364.
[5] J.H. Kaplan, Biochemistry of Na,K-ATPase, Annu. Rev. Biochem. 71 (2002) 511–535.
[6] G. Inesi, M. Kurzmack, C. Coan, D.E. Lewis, Cooperative calcium binding and ATPase activation in sarcoplasmic reticulum vesicles, J. Biol. Chem. 255 (1980) 3025–3031.
[7] C. Toyoshima, Structural aspects of ion pumping by Ca^{2+}-ATPase of sarcoplasmic reticulum, Arch. Biochem. Biophys. 476 (2008) 3–11.
[8] X. Yu, S. Carroll, J.L. Rigaud, G. Inesi, H^+ countertransport and electrogenicity of the sarcoplasmic reticulum Ca^{2+} pump in reconstituted proteoliposomes, Biophys. J. 64 (1993) 1232–1242.
[9] D.C. Gadsby, Ion pumps made crystal clear, Nature 450 (2007) 957–959.
[10] I. Prassas, E.P. Diamandis, Novel therapeutic applications of cardiac glycosides, Nature Review Drug Discovery 7 (2008) 926–935.
[11] C.R.D. Lancaster, A P-type ion pump at work, Nature Struct. Biol. 9 (2002) 643–645.
[12] J.M. Shin, K. Munson, O. Vagin, G. Sachs, The gastric HK-ATPase: structure, function, and inhibition, Europ. J. Phys. 457 (2009) 609–622.
[13] L. De Meis, A.L. Vianna, Energy interconversion by the Ca^{2+}-dependent ATPase of the sarcoplasmic reticulum, Ann. Rev. Biochem. 48 (1979) 275–292.
[14] R.W. Albers, Biochemical aspects of active transport, Ann. Rec. Biochem. 36 (1967) 727–756.
[15] R.L. Post, C. Hegyvary, S. Kume, Activation by adenosine triphosphate in the phosphorylation kinetics of sodium and potassium ion transport adenosine triphosphatase, J. Biol. Chem. 247 (1972) 6530–6540.
[16] C. Toyoshima, G. Inesi, Structural basis of ion pumping by Ca^{2+}-ATPase of the sarcoplasmic reticulum, Ann. Rev. Biochem. 73 (2004) 69–72.
[17] Z. Zhang, D. Lewis, C. Strock, G. Inesi, Detailed characterization of the cooperative mechanism of Ca^{2+} binding and catalytic activation in the Ca^{2+} transport (SERCA) ATPase, Biochem. 39 (2000) 8758–8767.
[18] R.B. Martin, Cooperative proton and calcium binding by sarcoplasmic reticulum ATPase, FEBS Lett. 308 (1992) 59–61.
[19] F. Tadini-Buoninsegni, G. Bartolommei, M.R. Moncelli, R. Guidelli, G. Inesi, Pre-steady state electrogenic events of Ca^{2+}/H^+ exchange and transport by the Ca^{2+}-ATPase, J. Biol. Chem. 281 (2006) 37720–37727.
[20] M. Chiesi, G. Inesi, Adenosine 5′-triphosphate dependent fluxes of manganese and hydrogen ions in sarcoplasmic reticulum vesicles, Biochem. 19 (1980) 2912–2928.

[21] V. Forge, E. Mintz, F. Guillain, Ca^{2+} binding to sarcoplasmic reticulum ATPase revisited. I. Mechanism of affinity and cooperativity modulation by H^+ and Mg^{2+}, J. Biol. Chem. 268 (1993) 10953–10960.
[22] R.J. Froud, A.G. Lee, Conformational transitions in the $Ca^{2+}+Mg^{2+}$-activated ATPase and the binding of Ca^{2+} ions, Biochem. 237 (1986) 197–206.
[23] J. Nakamura, Two types of proton-modulated calcium binding in the sarcoplasmic reticulum Ca^{2+}-ATPase. II. Characteristics of their calcium bindings, J. Biol. Chem. 269 (1994) 30822–30827.
[24] C. Peinelt, H.-J. Apell, Kinetics of the Ca^{2+}, H^+, and Mg^{2+} interaction with the ion-binding sites of the SR Ca-ATPase, Biophys. J. 82 (2002) 170–181.
[25] T. Daiho, K. Yamasaki, S. Danko, H. Suzuki, Critical role of Glu40-Ser48 loop linking actuator domain and the first transmembrane helix of Ca^{2+}-ATPase in Ca^{2+} deocclusion and release from ADP-insensitive phosphoenzyme, J. Biol. Chem. 282 (2007) 34429–34447.
[26] A.M. Hanel, W.P. Jencks, Dissociation of calcium from the phosphorylated calcium-transporting adenosine triphosphatase of sarcoplasmic reticulum: kinetic equivalence of the calcium ions bound to the phosphorylated enzyme. Biochem. 30 (1991) 11320–11330.
[27] S. Orlowski, P. Champeil, The two calcium ions initially bound to nonphosphorylated sarcoplasmic reticulum calcium ATPase can no longer be kinetically distinguished when they dissociate from phosphorylated ATPase toward the lumen. Biochem. 30 (1991) 11331–11342.
[28] F.T. Buoinsegni, G. Bartolommei, M.R. Moncelli, G. Inesi, R. Guidelli, Time-resolved charge translocation by sarcoplasmic reticulum Ca-ATPase measured on a solid supported membrane, Biophys. J. 86 (2004) 3671–3686.
[29] M. Yamaguchi, T. Kanazawa, Coincidence of H^+ binding and Ca^{2+} dissociation in the sarcoplasmic reticulum Ca-ATPase during ATP hydrolysis, J. Biol. Chem. (1985) 4896–4900.
[30] N. Stahl, W.P. Jencks, Reactions of the sarcoplasmic reticulum calcium adenosine triphosphatase with adenosine 5′-triphosphate and calcium that are not satisfactorily described by an E1–E2 model, Biochem. 26 (1987) 7654–7667.
[31] D.L. Stokes, N.M. Green, Structure and function of the calcium pump, Annu. Rev. Biophys. Biomol. Struct. 32 (2003) 446–468.
[32] J.V. Moller, P. Nissen, T.L.M. Sorensen, M. le Maire, Transport mechanism of the sarcoplasmic reticulum Ca^{2+}-ATPase pump, Curr. Opin. Struct. Biol. 15 (2005) 387–393.
[33] W. Hasselbach, W. Waas, Energy coupling in sarcoplasmic reticulum Ca^{2+} transport: an overview, Ann. N.Y. Acad. Sci. 402 (1982) 459–469.
[34] E. Mintz, F. Guillain, Ca^{2+} transport by the sarcoplasmic reticulum ATPase, Biochim. Biophys. Acta 1318 (1997) 52–70.
[35] N.M. Green, D.H. MacLennan, Calcium callisthenics, Nature 418 (2002) 598–599.
[36] A.G. Lee, J.M. East, What the structure of a calcium pump tells us about its mechanism, Biochem. J. 356 (2001) 665–683.
[37] A. Barth, Structural dynamics of the Ca^{2+}-ATPase studied by time-resolved infrared spectroscopy, Spectroscopy 22 (2008) 63–82.
[38] K.J. Sweadner, C. Donnet, Structural similarities of Na, K-ATPase and SERCA, the Ca^{2+}-ATPase of the sarcoplasmic reticulum, Biochem. J. 356 (2001) 685–704.
[39] N. Reyes, D.C. Gadsby, Ion permeation through the Na^+,K^+-ATPase, Nature Lett. 443 (2006) 470–474.
[40] A. Takeuchi, N. Reyes, P. Artigas, D.C. Gadsby, The ion pathway through the opened Na^+,K^+-ATPase pump, Nature 456 (2008) 413–416.
[41] J.B. Lingrel, T. Kuntzweiler, Na^+,K^+-ATPase, J. Biol. Chem. 269 (1994) 19659–19662.
[42] P.L. Jorgensen, K.O. Hakansson, S.J.D. Karlish, Structure and mechanism of Na,K-ATPase: functional sites and their interactions, Ann. Rev. Phys. 65 (2003) 817–849.
[43] C. Toyoshima, M. Nakasako, H. Nomura, T. Oka, Crystal structure of the calcium pump of sarcoplasmic reticulum at 2.6 A resolution, Nature 405 (2000) 647–655.
[44] C. Toyoshima, H. Nomura, Structural changes in the calcium pump accompanying the dissociation of calcium, Nature 418 (2002) 605–611.
[45] C. Toyoshima, T. Mizutani, Crystal structure of the calcium pump with a bound ATP analogue, Nature 430 (2004) 529–535.
[46] C. Toyoshima, H. Nomura, T. Tsuda, Lumenal gating mechanism revealed in calcium pump crystal structures with phosphate analogues, Nature 432 (2004) 361–368.
[47] C. Toyoshima, Y. Norimatsu, S. Iwasawa, T. Tsuda, H. Ogawa, How processing of aspartylphosphate is coupled to lumenal gating of the ion pathway in the calcium pump, Proc. Natl. Acad. Sci. U. S. A. 104 (2007) 19831–19836.
[48] C. Olesen, T.L.M. Sorensen, R.C. Nielsen, J.V. Moller, P. Nissen, Dephosphorylation of the calcium pump coupled to counterion occlusion, Science 306 (2004) 2251–2255.
[49] C. Olesen, M. Picard, A.M.L. Winther, C. Gyrup, J.P. Morth, C. Oxvig, J.V. Moller, P. Nissen, The structural basis of calcium transport by the calcium pump, Nature 450 (2007) 1036–1042.
[50] A.M.L. Jensen, T.L.M. Sorensen, C. Olesen, J.V. Moller, P. Nissen, Modulatory and catalytic modes of ATP binding by the calcium pump, EMBO J. 25 (2006) 2305–2314.
[51] J.P. Morth, B.P. Pedersen, M.S. Toustrup-Jensen, T.L.M. Sorensen, J. Petersen, J.P. Andersen, B. Vilsen, P. Nissen, Crystal structure of the sodium–potassium pump, Nature 450 (2007) 1043–1050.
[52] Anonymous, Calcium binding to the transmembrane domain of the sarcoplasmic reticulum Ca^{2+}-ATPase: insights from molecular modeling, Proteins 50 (2003) 104–113.
[53] M. Lape, C. Elam, M. Versluis, R. Kempton, S. Paula, Molecular determinants of sarco/endoplasmic reticulum calcium ATPase inhibition by hydroquinone-based compounds, Proteins-Structure Function and Bioinformatics 70 (2008) 639–649.
[54] N. Reuter, K. Hinsen, J.J. Lacapere, Transconformations of the SERCA1 Ca-ATPase: a normal mode study, Biophys. J. 85 (2003) 2186–2197.
[55] T.V. Pyrkov, Y.A. Kosinsky, A.S. Arseniev, J.P. Priestle, E. Jacoby, R.G. Efremov, Docking of ATP to Ca-ATPase: considering protein domain motions, Journal of Chemical Information and Modeling 47 (2007) 1171–1181.
[56] G. Li, Q. Cui, A coarse-grained normal mode approach for macromolecules: an efficient implementation and application for Ca^{2+}-ATPase, Biophys. J. 83 (2002) 2457–2474.
[57] D.L. Winters, J.M. Autry, B. Svensson, D.D. Thomas, Interdomain fluorescence resonance energy transfer in SERCA probed by cyan-fluorescent protein fused to the actuator domain, Biochem. 47 (2008) 4246–4256.
[58] R.J. Law, K. Munson, G. Sachs, F.C. Lightstone, An ion gating mechanism of gastric H,K-ATPase based on molecular dynamics simulations, Biophys. J. 95 (2008) 2739–2749.
[59] M. Morii, M. Yamauchi, T. Ichikawa, T. Fujii, Y. Takahashi, S. Asano, N. Takeguchi, H. Sakai, Involvement of the $H3O^+$-Lys-164-Gln-161-Glu-345 charge transfer pathway in proton transport of gastric H^+, K^+-ATPase, J. Biol. Chem. 283 (2008) 16876–16884.
[60] D. Bedeaux, S. Kjelstrup, The measurable heat flux that accompanies active transport by Ca^{2+}-ATPase, Phys. Chem. Chem. Phys. 10 (2008) 7304–7317.
[61] S. Kjelstrup, L. de Meis, D. Bedeaux, J.M. Simon, Is the Ca^{2+}-ATPase from sarcoplasmic reticulum also a heat pump? Eur. Biophys. J. 38 (2008) 59–67.
[62] Y. Sugita, N. Miyashita, M. Ikeguchi, A. Kidera, C. Toyoshima, Protonation of the acidic residues in the transmembrane cation-binding sites of the Ca^{2+} pump (2005) 6150–6151.
[63] K. Obara, N. Miyashita, C. Xu, I. Toyoshima, Y. Sugita, G. Inesi, C. Toyoshima, Structural role of countertransport revealed in Ca^{2+} pump crystal structure in the absence of Ca^{2+}, Proc. Natl. Acad. Sci. U. S. A. 102 (2005) 14489–14496.
[64] K. Hauser, Electrostatic calculations for assignment of IR difference bands to carboxyl groups getting protonated during protein reactions, Biopol. 82 (2006) 430–434.
[65] J. Andersson, K. Hauser, E.L. Karjalainen, A. Barth, Protonation and hydrogen bonding of Ca^{2+} site residues in the E2P phosphoenzyme intermediate of sarcoplasmic reticulum Ca^{2+}-ATPase studied by a combination of infrared experiments and electrostatic calculations, Biophys. J. 94 (2008) 600–611.
[66] E.-L. Karjalainen, K. Hauser, A. Barth, Proton paths in the sarcoplasmic reticulum Ca^{2+}-ATPase, Biochim.Biophys. Acta - Bioenergetics 1767 (2007) 1310–1318.
[67] K. Hauser, A. Barth, Side chain protonation and mobility in the sarcoplasmic reticulum Ca^{2+}-ATPase. Implications for proton countertransport and Ca^{2+} release, Biophys. J. 93 (2007) 3259–3270.
[68] C. Weidemüller, K. Hauser, Impact of an electric field on P-type ATPases, Spectroscopy 22 (2008) 319–325.
[69] C. Weidemüller, K. Hauser, in: U.H.E. Hansmann, J.H. Meinke, S. Mohanty, W. Nadler, O. Zimmermann (Eds.), A Computational Approach to Study the Energy Transduction Mechanism in the Na^+/K^+-ATPase, 40, John von Neumann Institute for Computing, Jülich, 2008, pp. 409–412.
[70] S. Geibel, J.H. Kaplan, E. Bamberg, T. Friedrich, Conformational dynamics of the Na^+/K^+-ATPase probed by voltage clamp fluorometry, Proc. Natl. Acad. Sci. U. S. A. 100 (2003) 964–969.
[71] R.E. Georgescu, E.G. Alexov, M.R. Gunner, Combining conformational flexibility and continuum electrostatics for calculating pKas in proteins, Biophys. J. 83 (2002) 1731–1748.
[72] E.G. Alexov, M.R. Gunner, Incorporating protein conformational flexibility into the calculation of pH-dependent protein properties, Biophys. J. 72 (1997) 2075–2093.
[73] M.R. Gunner, E.G. Alexov, A pragmatic approach to structure based calculation of coupled proton and electron transfer in proteins, Biochim. Biophys. Acta 1458 (2000) 63–87.
[74] J. Mao, K. Hauser, M.R. Gunner, How cytochromes with different folds control heme redox potentials, Biochem. 42 (2003) 9829–9840.
[75] K. Hauser, J. Mao, M.R. Gunner, pH dependence of heme electrochemistry in cytochromes investigated by multiconformation continuum electrostatic calculations, Biopol. 74 (2004) 51–54.
[76] Y. Song, J. Mao, M.R. Gunner, Calculation of proton transfer in bacteriorhodopsin bR and M intermediates, Biochem. 42 (2003) 9875–9888.
[77] Z.Y. Zhu, M.R. Gunner, Energetics of quinone-dependent electron transfers in *Rhodobacter sphaeroides* photosynthetic reaction centers, Biochem. 44 (2005) 82–96.
[78] J. Kim, J. Mao, M.R. Gunner, Are acidic and basic groups in buried proteins predicted to be ionized? J. Mol. Biol. (2005) 1283–1298.
[79] A. Nicholls, B. Honig, A rapid finite difference algorithm utilizing successive over-relaxation to solve the Poisson–Boltzmann equation, J. Comp. Chem. 12 (1991) 435–445.
[80] D. Sitkoff, K.A. Sharp, B. Honig, Accurate calculation of hydration free energies using of macroscopic solvent models, J. Phys. Chem. 98 (1994) 1978–1988.
[81] B. Boeckmann, A. Bairoch, R. Apweiler, M.C. Blatter, A. Estreicher, E. Gasteiger, M.J. Martin, K. Michoud, C. O'Donovan, I. Phan, S. Pilbout, M. Schneider, The SWISS-PROT protein knowledgebase and its supplement TrEMBL in 2003, Nucleic Acids Research 31 (2003) 365–370.
[82] W. Humphrey, A. Dalke, K. Schulten, VMD: visual molecular dynamics, J. Mol. Graph. 14 (1996) 33–38.
[83] J.C. Phillips, R. Braun, W. Wang, J. Gumbart, E. Tajkhorshid, E. Villa, C. Chipot, R.D. Skeel, L. Kale, K. Schulten, Scalable molecular dynamics with NAMD, J.of Comp. Chem. 26 (2005) 1781–1802.
[84] D. Levy, M. Seigneuret, A. Bluzat, J.L. Rigaud, Evidence for proton countertransport by sarcoplasmic reticulum Ca^{2+}-ATPase during calcium transport in reconstituted proteoliposomes with low ionic permeability, J. Biol. Chem. 265 (1990) 19524–19534.
[85] A.G. Da Costa, V.M.C. Madeira, Proton ejection as a major feature of the Ca^{2+} pump, Biochim. Biophys. Acta 1189 (1994) 181–188.

[86] X. Yu, L. Hao, G. Inesi, A pK change of acidic residues contributes to cation countertransport in the Ca-ATPase of sarcoplasmic reticulum, J. Biol. Chem. 269 (1994) 16656–16661.
[87] A. Barth, The infrared absorption of amino acid side chains, Progr. Biophys. Mol. Biol. (2000) 141–173.
[88] A.K. Dioumaev, Infrared methods for monitoring the protonation state of carboxyl amino acids in the photocycle of bacteriorhodopsin, Biochem. (Moscow) 66 (2001) 1269–1276.
[89] G.A. Scarborough, Molecular mechanism of the P-type ATPases, J. Bioenerg. Biomembr. 34 (2002) 235–250.
[90] S. Lutsenko, R. Anderko, J.H. Kaplan, Membrane disposition of the M5–M6 hairpin of Na^+,K^+-ATPase a subunit is ligand dependent, Proc. Natl. Acad. Sci. U. S. A. 92 (1995) 7936–7940.
[91] C. Gatto, S. Lutsenko, J.M. Sgin, G. Sachs, J.H. Kaplan, Stabilization of the H,K-ATPase M5M6 membrane hairpin by K^+ ions, J. Biol. Chem. 274 (1999) 13737–13740.
[92] T.L.M. Sorensen, J.P. Andersen, Importance of stalk segment S5 for intramolecular communication in the sarcoplasmic reticulum Ca^{2+}-ATPase, J. Biol. Chem. 275 (2000) 28954–28961.
[93] J.P. Andersen, Dissection of the functional domains of the sarcoplasmic reticulum Ca^{2+}-ATPase by site-directed mutagenesis, Biosci. Rep. 15 (1995) 243–261.
[94] D.B. Wells, V. Abramkina, A. Aksimentiev, Exploring transmembrane transport through α-hemolysin with grid-steered molecular dynamics, J. Chem. Phys. 127 (2007) 125101–1–125101–10.
[95] B. Roux, The membrane potential and its representation by a constant electric field in computer simulations, Biophys. J. 95 (2008) 4205–4216.
[96] R.J. Clarke, The dipole potential of phospholipid membranes and methods for its detection, Adv. Coll. Interf. Sci. 89–90 (2001) 263–281.
[97] T.L.M. Sorensen, J.V. Moller, P. Nissen, Phosphoryl transfer and calcium occlusion in the calcium pump, Science 304 (2004) 1672–1675.